Stability of PV-Hydrogen Energy Hubs with Grid-Forming Energy Storage

Yang, Fan; Yu, Haoyuan; Xiao, Junjie; Bauer, Pavol; Qin, Zian; Ganesh, Saran; Sharma, Toshi; Sahoo, Amulya; Lunshof, Martijn; Van Kruijsdijk, Cor

DOI
10.1109/PEDG62294.2025.11060378

Publication date
2025

Document Version
Final published version

Published in
PEDG 2025 - 2025 IEEE 16th International Symposium on Power Electronics for Distributed Generation Systems

Citation (APA)
Yang, F., Yu, H., Xiao, J., Bauer, P., Qin, Z., Ganesh, S., Sharma, T., Sahoo, A., Lunshof, M., & Van Kruijsdijk, C. (2025). Stability of PV-Hydrogen Energy Hubs with Grid-Forming Energy Storage. In *PEDG 2025 - 2025 IEEE 16th International Symposium on Power Electronics for Distributed Generation Systems* (pp. 539-544). (PEDG 2025 - 2025 IEEE 16th International Symposium on Power Electronics for Distributed Generation Systems). IEEE. https://doi.org/10.1109/PEDG62294.2025.11060378

2025 IEEE 16th International Symposium on Power Electronics for Distributed Generation Systems (PEDG) | 979-8-3315-8549-5/25/$31.00 ©2025 IEEE | DOI: 10.1109/PEDG62294.2025.11060378

Stability of PV-Hydrogen Energy Hubs with Grid-forming Energy Storage

Fan Yang, Haoyuan Yu, Junjie Xiao, Pavol Bauer, Zian Qin
Department of Electrical Sustainable Energy
Delft University of Technology, Delft,The Netherlands
Emails: {F.Y.Yang-1, H.Yu-6, J.Xiao-2, P.Bauer, Z.Qin-2}@tudelft.nl

Saran Ganesh, Toshi Sharma, Amulya Sahoo, Martijn Lunshof, Cor van Kruijsdijk
Shell Global Solutions International B.V.

Emails: {saran.ganesh, toshi.sharma, a.sahoo, m.lunshof, cor.vankruijsdijk}@shell.com

***Abstract*—Highly self-sufficient energy hubs offer a promising solution to mitigate grid congestion in favor of grid operators and to reduce grid fees for the benefit of energy hub operators. Meanwhile, the energy hub's capacity may far exceed the grid connection capacity, creating a weak grid situation. As a result, power quality issues such as voltage fluctuations, frequency deviations, and even instability may occur. In this work, a grid-forming energy storage system (GFM-ESS) is integrated to address these potential problems. A model of the GFM-ESS and energy hub is established based on a 50 kW PV-Hydrogen energy hub demonstrator, where PV-generated power is utilized for green hydrogen production. A trade-off design is proposed to identify the optimal balance between the capacity of the GFM-ESS and the grid connection. The voltage and frequency response at the hub's bus are analyzed to evaluate this trade-off. While experiments with the 50 kW demonstrator are ongoing, simulation results are provided to validate the effectiveness of the proposed design.**

***Index Terms*—energy hub, green hydrogen , GFM-ESS, Trade-off design, system stability**

I. Introduction

Green hydrogen, produced through water electrolysis, is gaining prominence in energy-intensive sectors such as chemical manufacturing and transportation. As a key energy carrier, it plays a crucial role in alleviating grid congestion caused by high-power-demand energy systems [1], [2]. To facilitate local energy production and consumption [3], the PV-Hydrogen energy hub concept—with limited grid connection capacity—offers a compelling approach to green hydrogen generation at a reduced Levelized Cost of Hydrogen (LCOH), thanks to significantly lowered grid fees. However, such setups create weak grid conditions, potentially jeopardizing the stability and power quality of the energy hub [4]. Compared to grid-following strategies, GFM-ESS is more suitable for weak grids, due to its voltage stiffness and inertia provisioning capabilities [5], [6].

The modern distribution network is expected to evolve into a flexibly coupled system interacting with the main grid, capable of actively supporting external power systems [3]. Energy hubs convert traditional distributed power supply architectures into integrated platforms that optimize the coordination among energy sources, grids, loads, and storage units, thereby enhancing the performance of distributed power systems.

A time-domain simulation model is implemented, balancing accuracy and computational efficiency by selecting and comparing techniques at both the power electronics [6] and system [7] levels. A well-parameterized demonstrator model is developed to validate the approach. A trade-off design is conducted to balance the capacities of the GFM-ESS and the grid connection. The energy hub's performance is tested under various GFM-ESS ratings and grid strengths, characterized by short-circuit ratios (SCR). Voltage and frequency responses are selected as key indicators of system stability. After careful tuning of current controllers and phase-locked loops [8], instability arises when the SCR drops below 1.5. Previous research [4] indicates that grid connections with SCR < 1.3 are difficult to stabilize under rated power conditions, despite extensive tuning.

This paper incorporates a GFM-controlled ESS, demonstrating the potential of hybrid energy storage in energy hubs. The GFM controller operates a lithium battery or supercapacitor [9] to support the grid. However, the addition of GFM-ESS increases system costs. Thus, a cost-performance trade-off design is introduced to balance installation costs and stability requirements, offering a practical pathway for energy hub implementation.

The remainder of the paper is structured as follows: Section II presents system parameters and configurations. Section III describes the control algorithms and modeling strategies. Section IV outlines test scenarios and simulation results. Section V concludes the paper.

II. System design and configurations

This section illustrates the design procedure of the energy hub, including energy components, power flow, electrical parameters, and protection schemes. Fig.1 shows the system configuration of the energy hub, including PV generation systems, GFM-ESS, and green hydrogen production systems. In this system, a PV system is the generation unit that produces green electricity. The electrolyzer consumes the energy produced by the PV system, generating green hydrogen. The external grid is connected to PCC by a short circuit limiter (SCLR) that forms different grid strength connections. GFM-ESS has been implemented to enhance the

stability of the system:

- A 50 kW PV inverter
- A 50 kW Green Hydrogen Electrolyzer
- An external grid connected with a short circuit limiter (SCLR)
- Energy storage system (ESS) for grid support

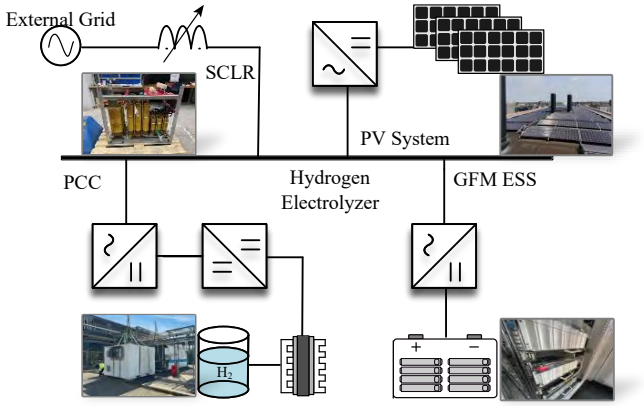

Fig. 1: The configuration of PV-Hydrogen energy hub.

A 50 kW photovoltaic battery provides solar power for the rectifier to electrolyze hydrogen. A short circuit limiter mimics the weak grid under different grid impedances. The consumption power from the electrolyzer is expected to be the same as the solar power, which achieves the localization of energy generation and consumption. As expected, the system becomes unstable if the external grid strength is reduced to SCR=1.5. The characteristic of this system is the combination of the external grid and GFM-ESS to stabilize the system. A trade-off design between the GFM-ESS rating and grid capacity is proposed and elaborated for the energy hub ESS configuration.

III. Modeling and Control

Inverter-based resource (IBR) control algorithms, such as grid-following (GFL) [10] and grid-forming (GFM) [11], are configured for the hydrogen electrolyzer and energy storage system, respectively. Voltage and frequency are selected as key indicators to reflect the system's stability performance under different test scenarios. The dynamic power flow of the PV source, electrolyzer load, external grid, and ESS is analyzed. Protection schemes such as current limiters and breakers are implemented to safeguard the inverters [12]. Finally, the PV-Hydrogen energy hub can operate in islanded mode with 100% local generation and consumption.

Proper modeling methods and control strategies must be designed for the energy hub. The converter models can be categorized as switching models, average models, and phasorial models, depending on the modeling depth. Although the switching model offers the highest accuracy by capturing switching behavior and power quality issues such as supraharmonics [13], it is computationally expensive at the system level. PSCAD is selected as the primary simulation tool due to its strong performance in electromagnetic transient (EMT) simulation. Furthermore, PSCAD's black-box capability makes it suitable for industrial use cases involving confidentiality concerns [14]. Table I summarizes the modeling types and control strategies used for each component.

TABLE I: Model Settings

Components	Control Strategy	Functions	Modeling type
External Grid	Voltage source	Grid strengths	EMT model
PV System	GFL Inverter	Energy provision	Average model
Electrolyzer	GFL rectifier	Load	Switching model
ESS	GFM Converter	Grid support	Average model

A. Grid Connection

The Grid capacity is defined by SCR (short circuit ratio). Eq. (1) defines the SCR, which varies from 5.0 to 0.5, by increasing the impedance of the short circuit limiter.

$$SCR = \frac{S_{sc}}{S_{rated}} = \frac{Z_{EH}}{Z_g} \tag{1}$$

S_{sc},S_{rated} are the short circuit power and rated power,Z_{EH},Z_g stands for the equivalent impedance of the energy hub and external grid. Besides, as the grid strength is reduced by increasing the inductance value of the SCLR, the line impedance can be considered as almost pure inductive, which gives the following eq.(2):

$$P = \frac{V_g V_c}{Z_g}(\theta_g - \theta_c) \quad Q = \frac{V_g V_c}{Z_g} - \frac{V_g^2}{Z_g} \tag{2}$$

P, Q is the active power and reactive power transmitted between the converter and the external grid. V_g, V_c are the grid and converter terminal voltages. Z_g is the grid impedance. Active power and reactive power decoupling are achieved by controlling the phase angle and voltage amplitude, respectively. GFM control aims to generate the θ_g and V_c signals to achieve grid synchronization.

B. Electrolyzer and PV

The electrolyzer model has three parts, including a GFL rectifier, a DC-DC step-down converter, and an Electrolyzer model. Fig.2 depicts the model and control of the rectifier and hydrogen electrolyzer, where a buck converter and a front-end rectifier supply the electrolyzer. The topology of the converter is a three-phase, two-level voltage source converter, which is described by eq.(3).

$$L\frac{di_d}{dt} = v_d - E_d + \omega_1 L i_q \quad L\frac{di_q}{dt} = v_q - E_q - \omega_1 L i_d \tag{3}$$

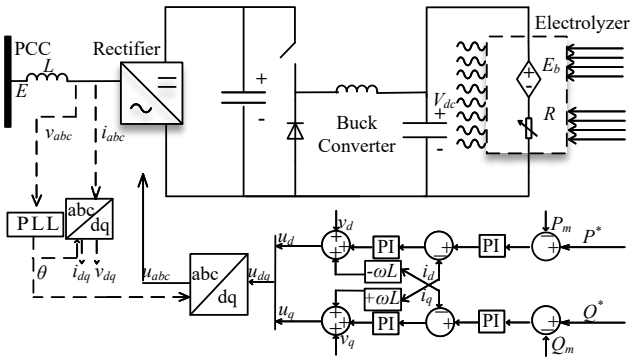

Fig. 2: Control of rectifier and hydrogen electrolyzer.

The control of the converter is a GFL rectifier power controller built-in DQ synchronous reference frame. Synchronous Reference Frame Phase-Locked Loop (SRF-PLL [15]) is implemented for grid synchronization. The controller is built in the cascaded structure. The outer loop is a power loop that generates the current reference signals, which are given by eq. (4).

$$(P^* - P)G_{pc} = i_d^* \quad (Q^* - Q)G_{pc} = i_q^* \tag{4}$$

G_{pc} is the power controller that generates the current reference signals i_d^* and i_q^*. P^* and Q^* are the active power setpoints and reactive power setpoints. The inner loop is the current controller that generates the voltage modulation signals. The current controller is built in the DQ axis by decoupling the DQ current. With the reference angle θ given by the PLL, reference voltage signals u_{abc} are obtained by conducting DQ inverse transformation, given in eq. (5).

$$u_d = (i_d^* - i_d)G_{cc} + v_d - \omega L i_q \quad u_q = (i_q^* - i_q)G_{cc} + v_q + \omega L i_d \tag{5}$$

u_d, u_q are given by the current controller and feed-forward compensation, which is computed by decoupling the DQ axis current. Power reference signal P^* is given by the measured output power P_{PV} to achieve instantaneous power tracking.

The function of the DC-DC Buck converter is to step down the voltage for the Electrolyzer. The loss is ignored for the DC-DC converter, which leads to the power balance given by eq. (6):

$$P_{EL} = P_{Rec} = P_{PV} \tag{6}$$

The Electrolyzer is modeled as a controlled voltage source series connected with a variable resistor [16]. The electrolyzing power is calculated by eq. (7).

$$P_{EL} = V_{dc}\frac{V_{dc} - E_b}{R} \tag{7}$$

Resistance R of the electrolyzer is referred to a look-up table, which is determined by the DC capacitor voltage V_{dc}. Hence, the consumption power of the electrolyzer is achieved by controlling the capacitor voltage V_{dc}. Besides, a short time transient is needed to charge the supercapacitor so that the capacitor voltage is higher than the back EMF. After that, the electrolysis process begins. The PV inverter control follows the same scheme as the Electrolyzer. A GFL inverter in power control mode is adopted to provide controlled power to the energy hub. The PV inverter's DC dynamics are modelled as a constant DC voltage source.

C. GFM-ESS

Fig.3 depicts the model and control of the ESS. A modified GFM droop control is implemented for the converter. LPF stands for the low-pass power filter.

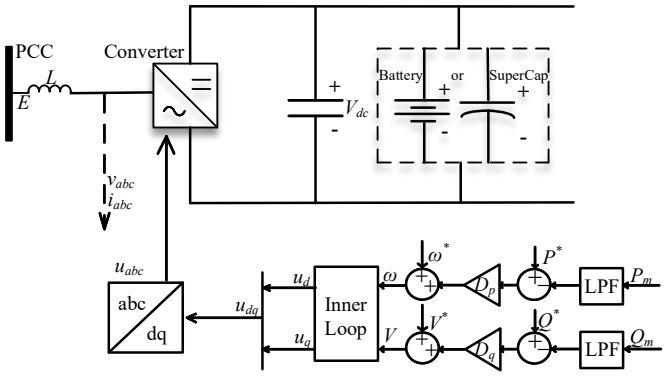

Fig. 3: ESS with GFM control

Eq. (8) calculates the measured power signals P_m and Q_m, which are filtered to get the feedback power signals P_f and Q_f.

$$P_f = \frac{1}{1+Ts}P_m \quad Q_f = \frac{1}{1+Ts}Q_m \tag{8}$$

In the GFM mode, the phase angle is given the integration of converter reference angular speed ω, derived from the active power droop control. The voltage reference signal V is derived by the reactive power droop. D_p and D_q stand for the active and reactive power droop coefficients, respectively. Eq.(9) gives the frequency and voltage reference signals, ω and V, respectively.

$$\omega = \omega^* + D_p(P^* - P_f) \quad V = V^* + D_q(Q^* - Q_f) \tag{9}$$

Substituting (8) into (9), the emulated inertia is given by $\frac{T}{D_p}$, while the damping is given by $\frac{1}{D_p}$, given as eq.(10).

$$\Delta\omega = \frac{1}{\frac{1}{D_p} + \frac{T}{Dp}s}\Delta P_m \tag{10}$$

Rewrite equation (10) as the Virtual Synchronous Machine (VSM) form to separate the inertia and damping power, which is given in equation (11). Emulated inertia and damping are given by M_c and D_c, shown as eq.(11).

$$\Delta\omega = \frac{1}{M_c s + D_c} = \frac{1}{\frac{1}{D_p} + \frac{T}{Dp}s}\Delta P_m \tag{11}$$

The GFM converter's power setpoint is set at zero, as solar power produces electrolyzing power. However, to maintain the energy hub's stable operation, a minimum capacity of the ESS size is required. Regarding the ESS storage components, the

battery is the conventional choice, and it can be considered a constant DC voltage source. However, the supercapacitor is more suitable for the ESS components in this energy hub. The difference between the supercapacitor and the battery is the regulation of the voltage of the DC side capacitor, which influences the modulation process. The modulation process of the converter is given by eq. (12).

$$d_{a,b,c} = \frac{u_{a,b,c}}{V_{dc}} \quad v_{a,b,c} = d_{a,b,c} V_{dc} \tag{12}$$

The modulation PWM signals $d_{a,b,c}$ for the three-phase two-level converters are generated by the modulation signals $u_{a,b,c}$. Then, the output three-phase voltage $v_{a,b,c}$ is obtained based on the modulation modes of the converter. Hence, if the overmodulation is avoided, both the battery and supercapacitor play the same function in the VSC control. Thus, the dynamics of the AC side and DC side are decoupled, which can be modeled separately. The supercapacitor is selected because of its high current capability compared to the constant power provision of a normal lithium battery. The model of the supercapacitor is simplified to the character of the capacitor shown as eq. (13).

$$V_{dc} = V_0 + \frac{1}{C_{cap}} \int i_c dt \tag{13}$$

V_0 is the initial voltage of the capacitor, C_{cap} is the capacitance of the supercapacitor. The supercapacitor model consists of many of the same submodels; a simplified model is used here to represent the system.

IV. The Proposed Trade-off Design of Energy Hub

With the completion of modeling, controller design, parameter tuning, and component selection for the demonstrator, the power allocation between the external grid and the GFM-ESS becomes a critical design task. The optimal configuration, or "sweet spot," minimizes both grid connection fees and the cost of ESS components while ensuring system stability.

A trade-off design approach is therefore proposed to weaken the grid connection progressively and assess the required power rating of the GFM-ESS, ensuring both voltage and frequency remain within acceptable limits. Fig. 4 illustrates the design process. The initial grid strength is set to SCR = 5, corresponding to a strong grid condition. The voltage and frequency deviations at the point of common coupling (PCC), denoted as ΔV_{pcc} and Δf_{pcc}, are selected as the stability indicators.

If the system performance satisfies these criteria, the SCR is decreased to emulate weaker grid conditions. If either voltage or frequency exceeds the operational range, the ESS capacity is increased. This iterative process continues until the SCR is reduced to zero, representing islanded operation. All tested grid strength conditions are recorded, and the associated grid and ESS costs are evaluated and compared. The configuration yielding the lowest total cost while maintaining stability is selected as the final design. Fig. 4 presents the flowchart of the proposed trade-off process

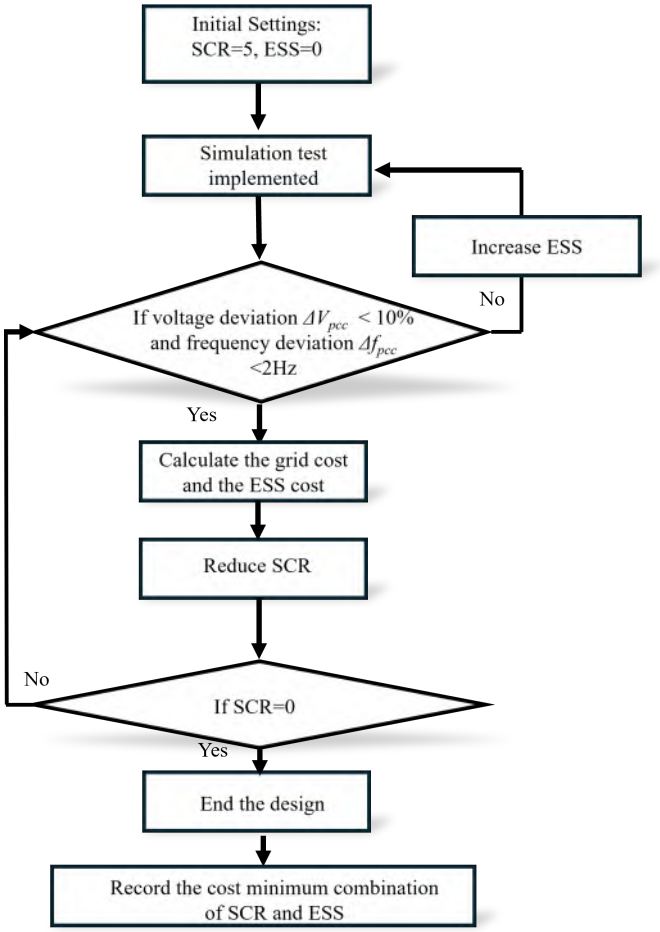

Fig. 4: The flow chart of the trade-off design process.

V. Scenario Tests and Simulations

The objective of these scenario tests is to evaluate the stability of the PV-Hydrogen Energy Hub under varying grid and ESS combinations, validating the proposed design process. Specifically, we analyze the impact of different grid strengths and energy storage capacities on system performance. A 50 kW PSCAD simulation model is developed to evaluate different scenarios. The simulation shows that SCR=1.5 is the boundary grid connection strength, which means a lower grid connection leads to instability. Table II presents the selected four simulation results.

TABLE II: Scenario Tests

Case	SCR	GFM-ESS(kVA)	V(%)	f(Hz)	Figure
1	1.5	0	±5%	±3.5	Fig.5
2	1.5	10	±3%	±0.5	Fig.6
3	0	10	±2.5%	±2.5	Fig.7
4	0	25	±1%	±0.5	Fig.8

Fig.5 presents the boundary grid strength condition without any grid support technologies which is of SCR=1.5. The solar power is set as a ramp signal to simulate the system response. It is inspected that the electrolyzer rectifier tracks the solar power after a short transient. At the time around 1s, the system

comes to a steady state. Although the system is stable, the frequency and voltage transients are still unaffordable for the Energy Hub, and GFM-ESS needs to be integrated to improve the stability performance.

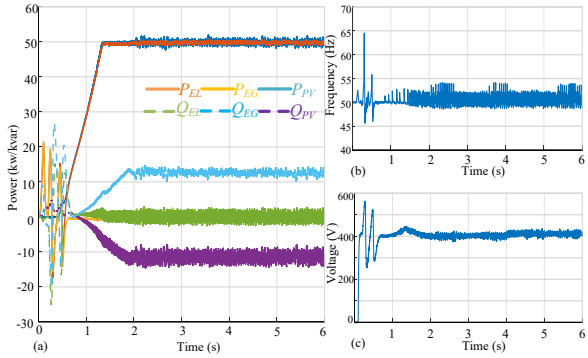

Fig. 5: Case 1: SCR=1.5, boundary condition without ESS support. The system is unstable if the SCR is less than 1.5. (a)Active and reactive power of the energy hub. (b) Frequency of the PCC. (c)Voltage amplitude of PCC.

Following the design procedure, the ESS is increased to maintain the voltage and frequency stability. Consequently, the GFM-ESS is increased to 10 kW, Fig. 6 presents the test results of the SCR=1.5 system with a GFM-ESS added. It is shown that the oscillations of active and reactive power curves are suppressed. The frequency is varied between ± 0.5 Hz, and the voltage is varied $\pm 3\%$ in the steady state.

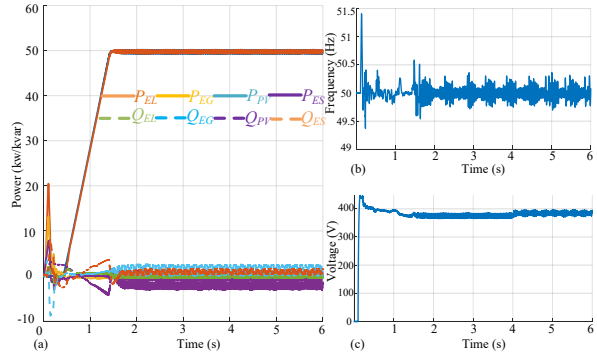

Fig. 6: Case 2: SCR=1.5 with a 10 kW GFM-ESS added. The system becomes stable again by integrating a 10 kW GFM ESS. (a)Active and reactive power of the energy hub. (b)Frequency of the PCC. (c)Voltage amplitude of PCC.

Continuing the design process until the SCR is decreased to 0. Fig. 7 presents a simulation test for a 10 kW-GFM ESS in the islanded mode. The Electrolyzer consumption tracks the solar generation power, which achieves the active power flow balance. Compared with fig.6, the absence of grid capacity leads to a small variation of the power curves. The frequency shows less desirable performance. However, the system is still working as expected, which is also a reasonable operation scenarios.

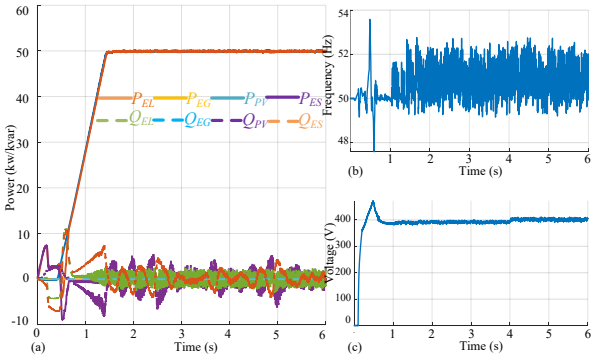

Fig. 7: Case 3: 10 kW ESS without grid connection. The voltage and frequency are out of operation range. (a)Active and reactive power of the Energy Hub. (b) Frequency of the PCC. (c)Voltage amplitude of PCC.

Finally, the GFM-ESS is enlarged to the maximum affordable design capacity, which is 25 kW, which provides the best voltage and frequency dynamics of in the islanded mode. From the simulation test shown in Fig. 8, the voltage is limited between 50 ± 0.5 Hz, which satisfies the European power system frequency operation requirements [17]. However, a 25 kW ESS might be too expensive and redundant for the system. The final decision is made considering the economic cost and the tolerance of energy hub equipment.

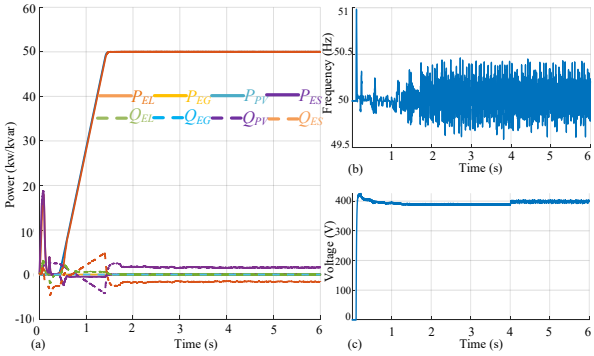

Fig. 8: Case 4: 25 kW GFM-ESS without grid connection. (a)Active and reactive power of the Energy Hub. (b) Frequency of the PCC. (c)Voltage amplitude of PCC.

VI. Conclusions

An Energy Hub design demonstrator, comprising a PV system, a hydrogen electrolyzer, and grid support components

such as a GFM-ESS, has been designed, modeled, and developed in this paper. Control algorithms including GFL control, droop control, and virtual synchronous machine (VSM) control are compared and implemented. A trade-off design is proposed to balance the grid connection strength and the power rating of the GFM-ESS. Simulations are conducted under various scenarios to validate the proposed methodology. The results demonstrate that a GFM-ESS with 20% of the rated capacity is sufficient to maintain the stability and power quality of a PV-Hydrogen Energy Hub. Finally, this paper presents a practical design demonstrator from a practical perspective, offering a new viewpoint on Energy Hub design.

REFERENCES

[1] M. Jayachandran, R. K. Gatla, A. Flah, A. H. Milyani, H. M. Milyani, V. Blazek, L. Prokop, and H. Kraiem, "Challenges and opportunities in green hydrogen adoption for decarbonizing hard-to-abate industries: A comprehensive review," *IEEE Access*, vol. 12, pp. 23 363–23 388, 2024.

[2] S. Chen, J. Zhang, Z. Wei, H. Cheng, and S. Lv, "Towards renewable-dominated energy systems: Role of green hydrogen," *Journal of Modern Power Systems and Clean Energy*, vol. 12, no. 6, pp. 1697–1709, 2024.

[3] S. Yinbiao, T. Yong, Z. Zhengling, Z. Fengying, Y. Lin, Z. Wuzhi, and G. Zhuoyuan, "Construction of new distribution network and its key technologies," *Proc. CSEE*, vol. 44, no. 17, pp. 6721–6732, September 2024.

[4] J. Z. Zhou, H. Ding, S. Fan, Y. Zhang, and A. M. Gole, "Impact of short-circuit ratio and phase-locked-loop parameters on the small-signal behavior of a vsc-hvdc converter," *IEEE Transactions on Power Delivery*, vol. 29, no. 5, pp. 2287–2296, 2014.

[5] D. B. Rathnayake, M. Akrami, C. Phurailatpam, S. P. Me, S. Hadavi, G. Jayasinghe, S. Zabihi, and B. Bahrani, "Grid forming inverter modeling, control, and applications," *IEEE Access*, vol. 9, pp. 114 781–114 807, 2021.

[6] G. De Carne, M. Langwasser, M. Ndreko, R. Bachmann, R. W. De Doncker, R. Dimitrovski, B. J. Mortimer, A. Neufeld, F. Rojas, and M. Liserre, "Which deepness class is suited for modeling power electronics?: A guide for choosing the right model for grid-integration studies," *IEEE Industrial Electronics Magazine*, vol. 13, no. 2, pp. 41–55, 2019.

[7] J. D. Lara, R. Henriquez-Auba, D. Ramasubramanian, S. Dhople, D. S. Callaway, and S. Sanders, "Revisiting power systems time-domain simulation methods and models," *IEEE Transactions on Power Systems*, vol. 39, no. 2, pp. 2421–2437, 2024.

[8] C. Li, S. Wang, and J. Liang, "Tuning method of a grid-following converter for the extremely-weak-grid connection," *IEEE Transactions on Power Systems*, vol. 37, no. 4, pp. 3169–3172, 2022.

[9] Skeleton Technologies, "Skelcap supercapacitors," 2024, available: https://www.skeletontech.com/en/skelcap-supercapacitors.

[10] J. Rocabert, A. Luna, F. Blaabjerg, and P. Rodríguez, "Control of power converters in ac microgrids," *IEEE Transactions on Power Electronics*, vol. 27, no. 11, pp. 4734–4749, 2012.

[11] W. Du, Z. Chen, K. P. Schneider, R. H. Lasseter, S. Pushpak Nandanoori, F. K. Tuffner, and S. Kundu, "A comparative study of two widely used grid-forming droop controls on microgrid small-signal stability," *IEEE Journal of Emerging and Selected Topics in Power Electronics*, vol. 8, no. 2, pp. 963–975, 2020.

[12] B. Fan, T. Liu, F. Zhao, H. Wu, and X. Wang, "A review of current-limiting control of grid-forming inverters under symmetrical disturbances," *IEEE Open Journal of Power Electronics*, vol. 3, pp. 955–969, 2022.

[13] L. Wang, Z. Qin, T. Slangen, P. Bauer, and T. van Wijk, "Grid impact of electric vehicle fast charging stations: Trends, standards, issues and mitigation measures - an overview," *IEEE Open Journal of Power Electronics*, vol. 2, pp. 56–74, 2021.

[14] PSCAD, "Blackboxing modules," PSCAD Online Help, 2024, available: https://www.pscad.com/webhelp-v502-ol/PSCAD/Features%20and%20Operations/Blackboxing%20Modules.htm.

[15] S.-K. Chung, "A phase tracking system for three phase utility interface inverters," *IEEE Transactions on Power Electronics*, vol. 15, no. 3, pp. 431–438, 2000.

[16] A. Ursúa and P. Sanchis, "Static–dynamic modelling of the electrical behaviour of a commercial advanced alkaline water electrolyser," *International Journal of Hydrogen Energy*, vol. 37, no. 24, pp. 18 598–18 614, 2012.

[17] ENTSO-E, "Guidance document for national implementation of frequency ranges for network codes on grid connection," ENTSO-E, Technical Report, April 2021, prepared from StG CNC.